Cramér-Rao Lower Bound for Power Line Integrated Communication and Sensing

Lutz Lampe
Department of Electrical and Computer Engineering,
The University of British Columbia, Vancouver, BC, Canada

***Abstract*—Power line communication (PLC) modems are transmitting high-frequency signals through the electric grid infrastructure. These signals can also be interpreted as probing or sensing signals. PLC is thus a natural candidate for integrated sensing and communication (ISAC). The implementation of grid sensing or monitoring with PLC has already been studied in previous work. In this paper, we ask the question what accuracy for (fault) parameter estimation can be achieved through power line ISAC. Since this is the first study of this kind, we are mainly concerned with introducing methodology. We adopt the Cramér-Rao lower bound (CRLB) as a performance criterion that is universally applicable regardless of the specific ISAC implementation. We show how to connect measurement variables and unknown parameters typically experienced in grid monitoring to obtain expressions for the CRLB. Using transmission-line modeling for PLC signal propagation, we identify automatic differentiation as a suitable tool to evaluate those expressions. The effectiveness of power line ISAC is illustrated through numerical results for a fault location estimation use case.**

***Index Terms*—Power line communication (PLC), integrated sensing and communication (ISAC), Cramér-Rao lower bound (CRLB), fault estimation, fault monitoring, smart grid, automatic differentiation.**

I. Introduction

The primary purpose of power lines is to transport and distribute electrical power. This is done by way of carrying electromagnetic waves at the 50 Hz or 60 Hz mains frequency. Naturally, power lines can also support waves at higher frequencies. When combined with modulating these high-frequency signals, this has given rise to power line communications (PLC) [1]. It is not surprising that the original use case for PLC was the support of power grid operations [1, Ch. 1]. This use case has experienced significant growth with the emergence of smart grids [2]. The growing need for reliable and fast communication to enable smart grid applications came along with advancements of PLC technology. As a result, the standardized physical layers of today's PLC modems (PLMs) are quite comparable to those in modern transceivers used for other communication media, such as wireless or coaxial or twisted pair cables [3].

PLC has been referred to as a reuse technique, as it exploits the existence of power lines to also transmit communication signals. On the other hand, one can also exploit the existence of communication signals sent between PLMs for the purpose of grid monitoring, e.g. [4], [5]. More specifically, PLMs can be seen as active (when sending and receiving PLC signals) or passive (when listening to power line noise) grid sensors. This means one can reuse already deployed PLC networks performing for example smart metering [6] for grid monitoring purposes. PLC therefore permits non-intrusive monitoring during regular grid operation and the transmission of raw or processed sensing data for further inference. Most of the literature on PLC-based monitoring has focused on fault detection and localization for overhead lines, e.g. [7], [8], and underground cables, e.g. [4], [5], [9]. Another trend especially in the more recent body of work is the use of machine learning to facilitate the detection and estimation in the case of model uncertainty, e.g., [4], [5], [9], [10].

The dual-function use of PLMs for communications and grid monitoring falls squarely into the area of integrated (or joint) sensing and communication (ISAC), which has garnered substantial interest in the wireless transmission domain, see [11] and references therein. One of the key aspects of ISAC lies in enabling the respective sensing and communication functionalities by the shared hardware resources. In the context of wireless ISAC, the sensing functionality usually refers to position and velocity estimation alike in radio detection and ranging (radar). In the context of power line ISAC, sensing can be applied to a broad spectrum of unknown quantities. These could relate to line and load parameters in normal grid operations, e.g., [12], parameters indicative for fault prediction, e.g., [4], [9], or parameters characterizing faults, e.g. [4], [5], [7], [8]. Reference [13] investigates how different categories of faults affect PLC signal propagation and provides guidelines to distinguish between them.

In this paper, we introduce a quantitative measure for the performance of sensing in power line ISAC. Specifically, we present the application of the Cramér-Rao lower bound (CRLB) [14, Ch. 3] to the estimation of fault parameters. This is similar to the use of the CRLB as a radar performance metric in wireless ISAC, e.g., [15]. We believe that this is the first work to apply the CRLB to power line ISAC. In particular, we introduce the mechanics of obtaining the CRLB for given sets of observed variables used for sensing and unknown parameters to be estimated. The observation variables suitable for inference are measurements of the network access impedance and the channel frequency response. The former corresponds to single-ended sensing using one PLM and the latter to double-ended sensing using two PLMs. Both quantities are already estimated in state-of-the-art PLMs for the purpose of data communication over the power line channel. One subtlety compared to conventional applications of CRLB [14, Ch. 3] is that we typically need to estimate

This work was supported by the Natural Sciences and Engineering Research Council of Canada (NSERC).

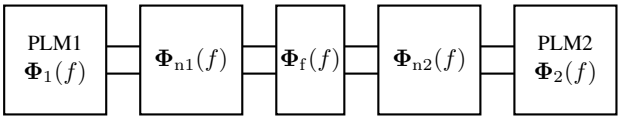

Fig. 1. Representation of the link between two PLMs using chain matrices.

complex parameters in power line ISAC. We make use of transmission-line models [16] to develop expressions for the Fisher information matrix (FIM) for combined complex and real unknown parameters and suggest the use of automatic differentiation [17] for their evaluation. We present numerical results for the task of locating a high-impedance fault along an underground power cable, using settings typical for a PLC system. Our results highlight the ability of power line ISAC for accurate location estimation and provide guidelines for the design of an effective ISAC scheme.

The remainder of this paper is organized as follows. In Section II, we describe the PLC signal propagation model using transmission line theory. The signal model is related to observations used for sensing in Section III. In Section IV, we introduce expressions for the FIM and thus the CRLB and the preferred method for their numerical evaluation. Numerical results for a fault location case are presented and discussed in Section V. Finally, we conclude in Section VI.

II. Signal Propagation Model

We consider a link between two PLMs using two conductors of transmission lines.[1] The grid components affecting the link between the two modems can be represented in the frequency domain through 2×2 chain parameter matrices $\mathbf{\Phi}(f) \in \mathbb{C}^{2\times 2}$ (see e.g. [16, Sec 6.5]) as shown in Figure 1, where $f \in \mathbb{R}$ denotes the frequency variable.

The representation in Figure 1 isolates the fault component with chain matrix $\mathbf{\Phi}_{\mathrm{f}}$ from the remainder of the network, where $\mathbf{\Phi}_{\mathrm{n1}}$ and $\mathbf{\Phi}_{\mathrm{n2}}$ represent the network components in the direction towards PLM1 and PLM2 from the fault location, respectively. $\mathbf{\Phi}_1$ and $\mathbf{\Phi}_2$ are the chain matrices for the two PLMs. The overall chain matrix between PLM1 and PLM2 is given by

$$\mathbf{\Phi}_{\mathrm{o}}(f) = \mathbf{\Phi}_1(f)\mathbf{\Phi}_{\mathrm{n1}}(f)\mathbf{\Phi}_{\mathrm{f}}(f)\mathbf{\Phi}_{\mathrm{n2}}(f)\mathbf{\Phi}_2(f)\ . \tag{1}$$

Example 1. As a concrete example, let us consider a transmission line network in which the two PLMs are connected via a power line of length L. PLM1 transmits with a source impedance Z_{s}, PLM2 receives with a load impedance Z_{r}, and the characteristic impedance and propagation constant of the line are Z_{c} and γ, respectively. Furthermore, we consider a high-impedance fault that puts an impedance Z_{f} between the two conductors. All variables are generally complex-valued and frequency-selective, i.e., functions that map from $f \in \mathbb{R}$ to $\mathbb{C}$. The corresponding chain matrices are

$$\mathbf{\Phi}_{\mathrm{n}i} = \begin{bmatrix} \cosh(\gamma\ell_i) & Z_{\mathrm{c}}\sinh(\gamma\ell_i) \\ Z_{\mathrm{c}}^{-1}\sinh(\gamma\ell_i) & \cosh(\gamma\ell_i) \end{bmatrix},\ i=1,2 \tag{2}$$

$$\mathbf{\Phi}_1 = \begin{bmatrix} 1 & Z_{\mathrm{s}} \\ 0 & 1 \end{bmatrix} \tag{3}$$

$$\mathbf{\Phi}_{\mathrm{f}} = \begin{bmatrix} 1 & 0 \\ Z_{\mathrm{f}}^{-1} & 1 \end{bmatrix} \tag{4}$$

$$\mathbf{\Phi}_2 = \begin{bmatrix} 1 & 0 \\ Z_{\mathrm{r}}^{-1} & 1 \end{bmatrix} \tag{5}$$

where we omitted the dependency on frequency f for compactness and ℓ_i denotes the length of the respective transmission line piece, i.e., $\ell_2 = L - \ell_1$.

III. Observation Model

PLMs routinely estimate the channel frequency response as well as the network access impedance. The former is part of the data detection process of PLMs providing moderate to high data rates [3]. These modems use multicarrier transmission and estimate the frequency response $H\colon \mathbb{R} \to \mathbb{C}$ at subcarrier frequencys f_k, $k \in \mathcal{K}$, where $\mathcal{K}$ is the set of used subcarriers. The access impedance $Z\colon \mathbb{R} \to \mathbb{C}$ can be measured similarly, usually with the purpose of adjusting the transmit power or facilitating in-band full duplexing [18], [19]. Writing the chain matrix as $\mathbf{\Phi}_{\mathrm{o}} = \begin{bmatrix} \Phi_{\mathrm{o},11} & \Phi_{\mathrm{o},12} \\ \Phi_{\mathrm{o},21} & \Phi_{\mathrm{o},22} \end{bmatrix}$ with elements $\Phi_{\mathrm{o},ij}$, we can express the frequency response for transmission from PLM1 to PLM2 as

$$H(f) = (\Phi_{\mathrm{o},11}(f))^{-1} \tag{6}$$

and the access impedance experienced at PLM1 as

$$Z(f) = \Phi_{\mathrm{o},11}(f)(\Phi_{\mathrm{o},21}(f))^{-1}. \tag{7}$$

The estimates $\hat{H}$ of the frequency response H and $\hat{Z}$ of the access impedance Z are the observation variables available to perform inference for the unknown fault-related parameters. To account for estimation errors, we use the measurement model

$$p_{\hat{H}(f)}(x) = \mathcal{CN}(x; H(f), \sigma_{\mathrm{h}}^2) \tag{8}$$

$$p_{\hat{Z}(f)}(x) = \mathcal{CN}(x; Z(f), \sigma_{\mathrm{z}}^2), \tag{9}$$

where $p_X\colon \mathbb{C} \to \mathbb{R}$ denotes the probability density function of the complex random variable X, and $\mathcal{CN}(x;\mu,\sigma^2)$ denotes the circularly symmetric complex Gaussian distribution with mean $\mu \in \mathbb{C}$ and variance $\sigma^2 \in \mathbb{R}$ evaluated at $x \in \mathbb{C}$. For simplicity, in this study we model the noise variances as frequency independent, while extensions could account for frequency dependence due to colored measurement noise in PLC links [20], [21].

The estimate $\hat{H}(f_m)$, $m \in \mathcal{M} \subseteq \mathcal{K}$, and $\hat{Z}(f_n)$, $n \in \mathcal{N} \subseteq \mathcal{K}$, that are used for inference are stacked into the vector of observations $\boldsymbol{X} \in \mathbb{C}^T$ of length $T = |\mathcal{M}|+|\mathcal{N}|$. The unknown quantities related to the fault can be a mix of p_{c} complex-valued parameters $\boldsymbol{\theta}_{\mathrm{c}}$ and p_{r} real-valued parameters $\boldsymbol{\theta}_{\mathrm{r}}$. We thus define the parameter vector $\boldsymbol{\theta} = \begin{bmatrix} \boldsymbol{\theta}_{\mathrm{c}} \\ \boldsymbol{\theta}_{\mathrm{r}} \end{bmatrix} \in \mathbb{C}^{p_{\mathrm{c}}} \times \mathbb{R}^{p_{\mathrm{r}}}$. We assume that the estimation-noise samples for the channel and

[1] The extension to multi-conductor PLC transmission is straightforward.

impedance measurements used for inference are statistically independent. Then, the resulting observation model connecting the observation and parameter vectors is given by

$$p_{\boldsymbol{X}}(\boldsymbol{x}) = \prod_{k=1}^{T} \mathcal{CN}(x_k; g_k(\boldsymbol{\theta}), \sigma_k^2), \tag{10}$$

where $g_k : \mathbb{C}^{p_\mathrm{c}} \times \mathbb{R}^{p_\mathrm{r}} \to \mathbb{C}$ depends on the model from Section II and $\sigma_k = \sigma_\mathrm{h}^2$ for $1 \le k \le |\mathcal{M}|$ and $\sigma_k = \sigma_\mathrm{z}^2$ for $|\mathcal{M}| < k \le T$.

Example 1. *(continued)* A typical task would be to identify the location, i.e., ℓ_1 or equivalently $\ell_2 = L - \ell_1$, and the severity, i.e., Z_f, of the fault. Then, and assuming that the line properties are known, $\boldsymbol{\theta} = [Z_\mathrm{f}, \ell_1]^\mathrm{T}$ and $p_\mathrm{c} = p_\mathrm{r} = 1$. Furthermore, considering (8) and (9), the function g_k in (10) is given by

$$g_k(\boldsymbol{\theta}) = \begin{cases} (\Phi_{\mathrm{o},11}(f_{m(k)}))^{-1}, & 1 \le k \le |\mathcal{M}| \\ \dfrac{\Phi_{\mathrm{o},11}(f_{m(k)})}{\Phi_{\mathrm{o},21}(f_{m(k)})}, & |\mathcal{M}| < k \le T \end{cases}$$

where $m(k)$ is the frequency index associated with the k-th observation and the $\Phi_{\mathrm{o},ij}$ need to be evaluated from (1) using (2)-(5).

IV. CRLB for Fault Parameter Estimation

In this section, we present the CRLB suitable for the sensing problems encountered in cable fault diagnostics by employing the observation model from Section III. Since the unknown parameters can be mixed real- and complex-valued quantities, we first introduce the application of the CRLB for complex parameters developed in [22]. Then we present a pragmatic approach to evaluate the CRLB expressions using the signal propagation model from Section II.

A. CRLB Expressions

A direct approach for the CRLB for complex parameters that does not require the expansion into real-valued vectors of stacked real and imaginary parts is described in [22]. It uses the extended parameter vector $\underline{\boldsymbol{\theta}} = \left[\boldsymbol{\theta}_\mathrm{c}^\mathrm{T}\ \boldsymbol{\theta}_\mathrm{c}^\mathrm{H}\ \boldsymbol{\theta}_\mathrm{r}^\mathrm{T}\right]^\mathrm{T}$ and the complex Fisher information matrix

$$\boldsymbol{I}(\underline{\boldsymbol{\theta}}) = \mathrm{E}\left[\left(\frac{\partial \log(p_{\boldsymbol{X}})}{\partial \underline{\boldsymbol{\theta}}}\right)^* \left(\frac{\partial \log(p_{\boldsymbol{X}})}{\partial \underline{\boldsymbol{\theta}}}\right)^\mathrm{T}\right] \tag{11}$$

to bound the covariance matrix of any unbiased estimator as [22, Th. 1]

$$\mathrm{E}\left[(\hat{\underline{\boldsymbol{\theta}}} - \underline{\boldsymbol{\theta}})(\hat{\underline{\boldsymbol{\theta}}} - \underline{\boldsymbol{\theta}})^\mathrm{H}\right] \ge \boldsymbol{I}(\underline{\boldsymbol{\theta}})^{-1}, \tag{12}$$

where E is the expectation operator and the matrix inequality $\boldsymbol{A} \ge \boldsymbol{B}$ means that $(\boldsymbol{A} - \boldsymbol{B})$ is positive semi-definite. In (11), we use the complex gradient [22, Def. 1]

$$\frac{\partial h}{\partial \underline{\boldsymbol{\theta}}} = \begin{bmatrix} \frac{\partial h}{\partial \boldsymbol{\theta}_\mathrm{c}} \\ \frac{\partial h}{\partial \boldsymbol{\theta}_\mathrm{c}^*} \\ \frac{\partial h}{\partial \boldsymbol{\theta}_\mathrm{r}} \end{bmatrix} \tag{13}$$

for any scalar function h. The derivatives with respect to complex variables $\boldsymbol{\theta}_\mathrm{c}$ and $\boldsymbol{\theta}_\mathrm{c}^*$ are evaluated using the Wirtinger calculus, which defines suitable differential operators for non-analytic functions [23, App. A].

Applying (11) to the observation model in (10) gives

$$\boldsymbol{I}(\underline{\boldsymbol{\theta}}) = \sum_{i=1}^{T}\sum_{j=1}^{T} \underbrace{\frac{1}{\sigma_i^2\sigma_j^2}\mathrm{E}\left[\left(\frac{\partial|x_i - g_i|^2}{\partial \underline{\boldsymbol{\theta}}}\right)^* \left(\frac{\partial|x_j - g_j|^2}{\underline{\boldsymbol{\theta}}}\right)^\mathrm{T}\right]}_{\boldsymbol{I}_{ij}(\underline{\boldsymbol{\theta}})}. \tag{14}$$

Since

$$\begin{aligned} \frac{\partial|x_i - g_i|^2}{\partial \underline{\boldsymbol{\theta}}} &= -(x_i - g_i(\boldsymbol{\theta}))\frac{\partial(x_i - g_i)^*}{\partial \underline{\boldsymbol{\theta}}} \\ &\quad -(x_i - g_i(\boldsymbol{\theta}))^*\frac{\partial(x_i - g_i)}{\partial \underline{\boldsymbol{\theta}}}, \end{aligned}$$

we can evaluate the summation terms $I_{ij}(\underline{\boldsymbol{\theta}})$ in (14) as

$$\begin{aligned} \boldsymbol{I}_{ij}(\underline{\boldsymbol{\theta}}) &= \frac{1}{\sigma_i^2\sigma_j^2}\mathrm{E}\Big[(x_i - g_i(\boldsymbol{\theta}))(x_j - g_j(\boldsymbol{\theta}))^*\boldsymbol{\Delta}_i^*\boldsymbol{\Delta}_j^\mathrm{T} \\ &\quad +(x_i - g_i(\boldsymbol{\theta}))(x_j - g_j(\boldsymbol{\theta}))\boldsymbol{\Delta}_i\tilde{\boldsymbol{\Delta}}_j^\mathrm{T} \\ &\quad +(x_i - g_i(\boldsymbol{\theta}))^*(x_j - g_j(\boldsymbol{\theta}))^*\tilde{\boldsymbol{\Delta}}_i^*\boldsymbol{\Delta}_j^\mathrm{T} \\ &\quad +(x_i - g_i(\boldsymbol{\theta}))^*(x_j - g_j(\boldsymbol{\theta}))\tilde{\boldsymbol{\Delta}}_i^*\tilde{\boldsymbol{\Delta}}_j^\mathrm{T}\Big] \\ &= \begin{cases} \boldsymbol{I}_i(\underline{\boldsymbol{\theta}}), & \text{if } i = j \\ 0, & \text{if } i \ne j \end{cases}, \end{aligned} \tag{15}$$

where $\boldsymbol{\Delta}_i = \frac{\partial g_i}{\partial \underline{\boldsymbol{\theta}}}$, $\tilde{\boldsymbol{\Delta}}_i = \frac{\partial g_i^*}{\partial \underline{\boldsymbol{\theta}}}$, and

$$\boldsymbol{I}_i(\underline{\boldsymbol{\theta}}) = \frac{1}{\sigma_i^4}\left[\boldsymbol{\Delta}_i^*\boldsymbol{\Delta}_i^\mathrm{T} + \tilde{\boldsymbol{\Delta}}_i^*\tilde{\boldsymbol{\Delta}}_i^\mathrm{T}\right]. \tag{16}$$

Accordingly, (14) simplifies to

$$\boldsymbol{I}(\underline{\boldsymbol{\theta}}) = \sum_{i=1}^{T}\boldsymbol{I}_i(\underline{\boldsymbol{\theta}}). \tag{17}$$

B. CRLB Evaluation

The evaluation of the expressions in (16) and (17) is conceptually straightforward. Since the functions g_k are computed using the transmission-line model in (1), their partial derivatives with respect to the fault parameters can be evaluated with the repeated use of the chain rule of derivatives.

Example 1. *(continued)* Let us consider the fault location ℓ_1 as a parameter of interest and the frequency response (8) as the kth component function g_k, $1 \le k \le |\mathcal{M}|$. Defining $\boldsymbol{a} = [1\ 0]^\mathrm{T}$ and dropping the dependency on the frequency $f_{m(k)}$ for brevity, the corresponding partial derivative can be evaluated as follows:

$$\begin{aligned} \frac{\partial g_k}{\partial \ell_1} &= \frac{\partial\left(\boldsymbol{a}^\mathrm{T}\boldsymbol{\Phi}_\mathrm{o}\boldsymbol{a}\right)^{-1}}{\partial \ell_1} \\ &= -\left(\boldsymbol{a}^\mathrm{T}\boldsymbol{\Phi}_\mathrm{o}\boldsymbol{a}\right)^{-2}\boldsymbol{a}^\mathrm{T}\frac{\partial\boldsymbol{\Phi}_\mathrm{o}}{\partial \ell_1}\boldsymbol{a} \\ &= -\left(\boldsymbol{a}^\mathrm{T}\boldsymbol{\Phi}_\mathrm{o}\boldsymbol{a}\right)^{-2}\boldsymbol{a}^\mathrm{T}\boldsymbol{\Phi}_1\frac{\partial\boldsymbol{\Phi}_{\mathrm{n}1}\boldsymbol{\Phi}_\mathrm{f}\boldsymbol{\Phi}_{\mathrm{n}2}}{\partial \ell_1}\boldsymbol{\Phi}_2\boldsymbol{a} \\ &= -\left(\boldsymbol{a}^T\boldsymbol{\Phi}_\mathrm{o}\boldsymbol{a}\right)^{-2}\boldsymbol{a}^T\boldsymbol{\Phi}_1\left[\frac{\partial\boldsymbol{\Phi}_{\mathrm{n}1}}{\partial \ell_1}\boldsymbol{\Phi}_\mathrm{f}\boldsymbol{\Phi}_{\mathrm{n}2}\right. \\ &\quad \left.+\boldsymbol{\Phi}_{\mathrm{n}1}\boldsymbol{\Phi}_\mathrm{f}\frac{\partial\boldsymbol{\Phi}_{\mathrm{n}2}}{\partial \ell_1}\right]\boldsymbol{\Phi}_2\boldsymbol{a}. \end{aligned} \tag{18}$$

TABLE I

AUTOMATIC DIFFERENTIATION FOR $\mathbf{\Phi}_{\mathrm{n1}}$ IN EQ. (2) USING THE COMPUTATIONAL GRAPH IN FIG. 2. THE NOTATION $\dot{v}_i = \frac{\partial v_i}{\partial \ell_1}$ IS USED. THE NUMERICAL VALUES ARE CHOSEN FOR SIMPLE ILLUSTRATION.

computation of $\mathbf{\Phi}_{\mathrm{n1}}$		computation of $\frac{\partial \mathbf{\Phi}_{\mathrm{n1}}}{\partial \ell_1}$	
$v_1 = \ell_1$	$= 1.0$	$\dot{v}_1 = \dot{\ell}_1$	$= 1.0$
$v_2 = \gamma$	$= 1.0$	$\dot{v}_2 = \dot{\gamma}$	$= 0$
$v_3 = Z_{\mathrm{c}}$	$= 0.5$	$\dot{v}_3 = \dot{Z}_{\mathrm{c}}$	$= 0$
$v_4 = v_2 v_1$	$= 1.0$	$\dot{v}_4 = \dot{v}_2 v_1 + \dot{v}_1 v_2$	$= 1.0$
$v_5 = \cosh(v_4)$	$= 1.5$	$\dot{v}_5 = \sinh(v_4)\dot{v}_4$	$= 1.2$
$v_6 = \sinh(v_4)$	$= 1.2$	$\dot{v}_6 = \cosh(v_4)\dot{v}_4$	$= 1.5$
$v_7 = v_3 v_6$	$= 0.6$	$\dot{v}_7 = \dot{v}_3 v_6 + \dot{v}_6 v_3$	$= 0.8$
$v_8 = v_6 / v_3$	$= 2.4$	$\dot{v}_8 = (\dot{v}_3 v_6 + \dot{v}_6 v_3)/v_3^2$	$= 3.1$
$\mathbf{\Phi}_{\mathrm{n1}} = v_9$		$\frac{\partial \mathbf{\Phi}_{\mathrm{n1}}}{\partial \ell_1} = \dot{v}_9$	
$= \begin{bmatrix} v_5 & v_7 \\ v_8 & v_5 \end{bmatrix}$	$= \begin{bmatrix} 1.5 & 0.6 \\ 2.4 & 1.5 \end{bmatrix}$	$= \begin{bmatrix} \dot{v}_5 & \dot{v}_7 \\ \dot{v}_8 & \dot{v}_5 \end{bmatrix}$	$= \begin{bmatrix} 1.2 & 0.8 \\ 3.1 & 1.2 \end{bmatrix}$

The partial derivatives in (18) require one more application of the chain rule and are elementary.

While the procedure illustrated in the example is generally applicable for the signal propagation model from Section II, it quickly becomes cumbersome and the final expressions become humongous when power line networks with more branches and loads are considered. An effective alternative to this symbolic differentiation is automatic differentiation [17]. Automatic differentiation computes derivatives alongside the computation of function values and provides accurate numerical results without the need for closed-form expressions. That is, when one computes for example the value H in (6) for given parameters $\boldsymbol{\theta}'$, then the values of the partial derivatives $\frac{\partial H}{\partial \boldsymbol{\theta}}\Big|_{\boldsymbol{\theta}=\boldsymbol{\theta}'}$ are also computed. Automatic differentiation is thus a meaningful approach if one is interested in quantitative results and not in analyzing trends based on a closed-form expression.

Example 1. *(continued)* We illustrate the steps of automatic differentiation until the computation of $\frac{\partial \mathbf{\Phi}_{\mathrm{n1}}}{\partial \ell_1}$ in (18). For this, we consider the forward mode automatic differentiation and follow the exposition in [17, Sec. 3.1]. Accordingly, we draw the computational graph in Fig. 2 representing the operations for the execution of (2) to compute $\mathbf{\Phi}_{\mathrm{n1}}$. The corresponding numerical calculations are given in the left-hand side of Table I. The first three rows are the initialization of the input parameters. The derivative $\frac{\partial \mathbf{\Phi}_{\mathrm{n1}}}{\partial \ell_1}$ is computed via automatic differentiation at the right-hand side of Table I.

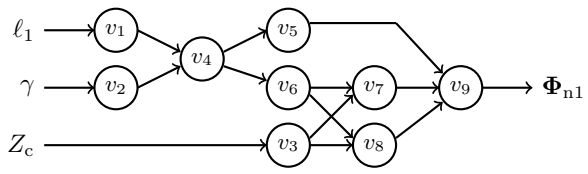

Fig. 2. Computational graph to compute $\mathbf{\Phi}_{\mathrm{n1}}$.

V. NUMERICAL RESULTS

We continue with the setting from Example 1 and evaluate the CRLB expressions for the case of a 1000 m long N2XSEY cable (see [4] for details) with a high-impedance fault Z_{f} at

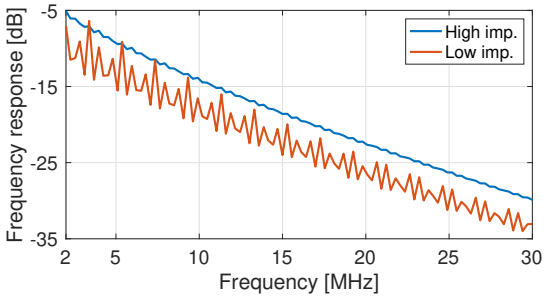

Fig. 3. Frequency response for the considered system with a high-impedance $Z_{\mathrm{f}} = (1000 + \mathrm{j}50)\ \Omega$ and low-impedance $Z_{\mathrm{f}} = (10 + \mathrm{j}50)\ \Omega$ fault.

$\ell_1 = 200$ m distance from PLM1. In the context of power line ISAC, we assume that the PLMs operate in the frequency range of 2-30 MHz and use multicarrier transmission with a subcarrier spacing of 24.4 kHz. Pilot signals at subsets of those subcarriers are used to obtain frequency response and access impedance measurements. The source impedance is $Z_{\mathrm{s}} = 5\ \Omega$ and the load impedance is set to $Z_{\mathrm{r}} = (100 - \mathrm{j}5)\ \Omega$, as low source and higher load impedance are typical for PLC.

Figure 3 shows the frequency response H from PLM1 to PLM2 when $Z_{\mathrm{f}} = (1000 + \mathrm{j}50)\ \Omega$ and $Z_{\mathrm{f}} = (10 + \mathrm{j}50)\ \Omega$, respectively. The former is a high-impedance fault and the frequency response is mostly that of a power cable causing higher signal attenuation with increasing frequency. The second case for Z_{f} is more a low-impedance fault, and one can observe ripples in the frequency response due to signal reflections at the location of the impedance. From this visual inspection of H, one would expect that it may be difficult to infer fault parameters for high-impedance faults with large resistance.

Throughout the following we focus on results for the task of identifying the location ℓ_1 of the fault. We expand the vector $\boldsymbol{\theta}$ of unknown parameters by unknown fault and load impedances, Z_{f} and Z_{r}, which are thus nuisance parameters.

A. Using Frequency Response

We start by using only the estimates of the frequency response H in (6) for inference. The variance σ_{h}^2 is adjusted according to a specified signal-to-noise ratio (SNR) $\sum_m |H(f_m) - \hat{H}(f_m)|^2/\sigma_{\mathrm{h}}^2$ for frequencies in the range $2 \le f_m \le 6$ MHz.

1) Unknown impedances are known to be constant: We first assume that the fault and load impedance are unknown but known to be frequency independent, i.e., $\boldsymbol{\theta} = [Z_{\mathrm{f}}, Z_{\mathrm{r}}, \ell_1]^{\mathrm{T}}$ with $p_{\mathrm{c}} = 2$, $p_{\mathrm{r}} = 1$.

Figure 4 shows the CRLB for the root mean square error (RMSE) versus the number of measurements T for $\hat{H}$ in the range of $2-28$ MHz used for location estimation of a fault with $Z_{\mathrm{f}} = (1000 + \mathrm{j}50)\ \Omega$. We observe that an estimation accuracy in the meter and even sub-meter range can be obtained if more than about 50 measurements are used at an SNR of 0 dB and 10 dB, respectively. These values demonstrate the potential for accurate fault localization using channel estimation based on PLC pilot signals.

In Figure 5 we inspect the role of the frequency range over which the pilots are distributed. The figure shows the

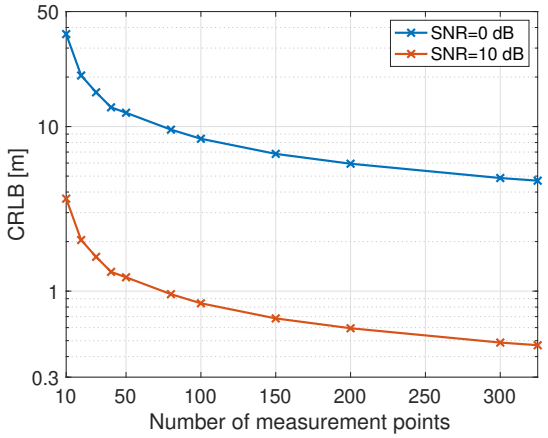

Fig. 4. CRLB as a function of the number of observation T. $\hat{H}$ in the frequency range from $2-28$ MHz is used, and $Z_{\mathrm{f}} = (1000 + \mathrm{j}50)\ \Omega$.

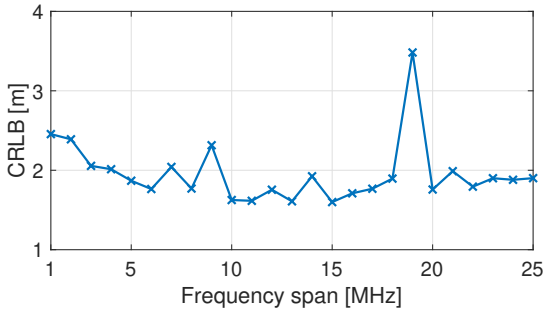

Fig. 5. CRLB as a function of the frequency span within which $T = 20$ observations are obtained. $\hat{H}$ is used. $Z_{\mathrm{f}} = (1000+\mathrm{j}50)\ \Omega$ and SNR$=10$ dB.

CRLB for $T = 20$ measurements for frequency spans from $B = 1$ MHz to $B = 25$ MHz, i.e., the PLMs operate in the frequency range from 2 MHz to $(B + 2)$ MHz. As it can be seen, the CRLB remains fairly constant at around 2-3 m for all frequency spans B. We attribute the fluctuations such as at $B = 19$ MHz to the specific frequency samples of H that are being used for location estimation, rather than the frequency span itself.

Next, we explore the sensitivity to the severity of the high-impedance fault. We fix the number of measurements to $T = 20$ and the frequency band to 2-6 MHz. Figure 6 shows the CRLB as a function of the fault resistance. As expected, the estimation accuracy is high for low resistance values but declines fairly steeply for high resistances above 1 kΩ. For further increasing resistance values above 10 kΩ (not shown), the CRLB may become useless, i.e., the estimation error exceeds the link length or the FIM becomes ill-conditioned and its inversion numerically unstable.

2) Unknown impedances are not assumed constant: It is likely too strong an idealization to assume that fault and load impedances are constant over the entire frequency range used for measurements. We therefore relax this constraint and adopt a piece-wise constant model. That is, we assume that there are $p_{\mathrm{c}} = 2U$ unknown impedances with $U \geq 1$, which are constant only over a coherence bandwidth which is the Uth fraction of the entire frequency band. Using $T = 100$ measurements $\hat{H}$ in the frequency band from $2-6$ MHz,

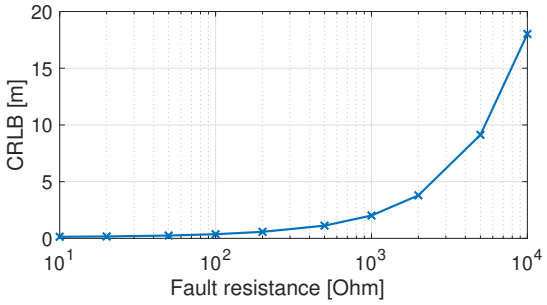

Fig. 6. CRLB as a function of the resistance of Z_{f}. Reactance is 50 Ω. $T = 20$ observations of $\hat{H}$ in $2-6$ MHz are used. SNR$=10$ dB.

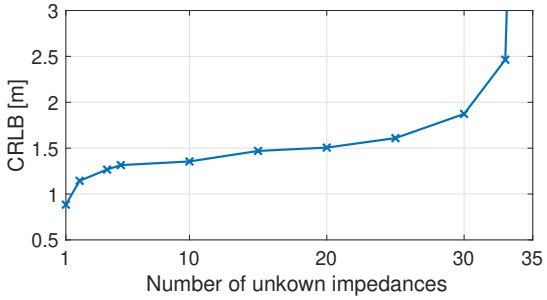

Fig. 7. CRLB as a function of the number U of unknown impedances in the frequency range. $T = 100$ observations of $\hat{H}$ in $2-6$ MHz are used. $Z_{\mathrm{f}} = (1000 + \mathrm{j}50)\ \Omega$ and SNR$=10$ dB.

Figure 7 shows the CRLB versus the number U. For those results, for consistency with the previously shown results, we keep the actual realizations of Z_{f} and Z_{r} frequency independent. However, the estimator needs to estimate $(2U + 1)$ unknown parameters $Z_{\mathrm{f}}(f)$, $Z_{\mathrm{r}}(f)$, and ℓ_1. We observe how the estimation accuracy deteriorates with increasing number of unknown impedances. While the degradation is fairly benign at first, beyond $U = 33$ the FIM becomes ill-conditioned and no meaningful results are obtained. The ratio between number of measurements T and number U of unknown impedances is important. The results in Figure 7 suggest $T/U \gtrsim 3$, i.e., three measurements per unknown parameters Z_{f} and Z_{r}, should be used.

B. Using Frequency Response and Network Impedance

Finally, we use estimates of the frequency response H in (6) and the network access impedance Z in (7) for inference. Figure 8 presents the results for the same setting as in Figure 7. We differentiate between the SNR for the channel frequency response estimation (SNR$_H$) and the SNR for the access impedance estimation (SNR$_Z$), according to which the variances σ_{h}^2 and σ_{z}^2 used in (16) as σ_i^2 are adjusted. First, we observe that the additional use of access-impedance estimations $\hat{Z}$ provides benefits for the case of a large number U of unknowns. This is because the ratio between the total number of measurements T and the number of unknowns is increased by a factor of two compared to only using $\hat{H}$. Secondly, there is little gain in estimation accuracy for smaller number of unknown parameters, unless the SNR for the estimation of access impedance is substantial larger

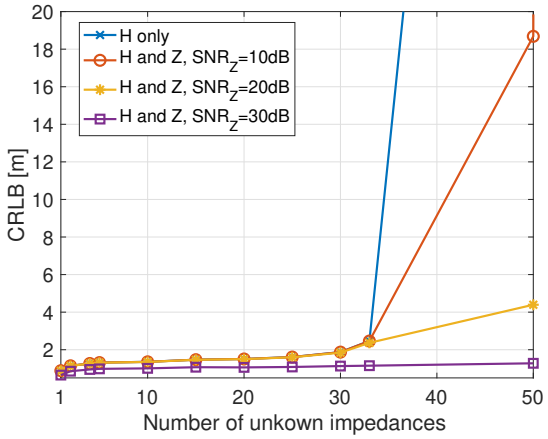

Fig. 8. CRLB as a function of the number U of unknown impedances in the frequency range. $T = 100$ observations of $\hat{H}$ and $\hat{Z}$ in $2-6$ MHz are used. $Z_{\mathrm{f}} = (1000 + \mathrm{j}50)\ \Omega$, $\mathrm{SNR}_H = 10$ dB, and $\mathrm{SNR}_Z = [10, 20, 30]$ dB.

than that for the estimation of channel frequency response. While this illustrates the potential benefit of using additional observations, it also suggests that the network impedance is less informative than the channel frequency response. This may be due to the differences between single-ended (network access impedance) versus double-ended (channel frequency response) sensing, and warrants further investigation.

VI. Conclusions

In this paper, we introduced the CRLB as a measure for sensing performance in power line ISAC. We believe that this is a new contribution that will support the development and analysis of grid monitoring solutions that exploit the through-the-grid property of PLC. Our work focused on the methodology for formulating and evaluating the CRLB. We applied our method to the use case of estimating the location of a high-impedance fault. The results highlight the potential of ISAC in achieving high estimation accuracy and shed light on the roles of system parameters for the estimation task. Future work will include the consideration of more complex power line networks and the extension to detection problems.

References

[1] L. Lampe, A. M. Tonello, and T. G. Swart, *Power Line Communications: Principles, Standards and Applications from multimedia to smart grid*. John Wiley & Sons, 2016.

[2] S. Galli, A. Scaglione, and Z. Wang, "For the grid and through the grid: The role of power line communications in the smart grid," *Proceedings of the IEEE*, vol. 99, no. 6, pp. 998–1027, 2011.

[3] C. Cano, A. Pittolo, D. Malone, L. Lampe, A. M. Tonello, and A. G. Dabak, "State of the art in power line communications: From the applications to the medium," *IEEE Journal on Selected Areas in Communications*, vol. 34, no. 7, pp. 1935–1952, 2016.

[4] Y. Huo, G. Prasad, L. Atanackovic, L. Lampe, and V. C. M. Leung, "Cable diagnostics with power line modems for smart grid monitoring," *IEEE Access*, vol. 7, pp. 60 206–60 220, 2019.

[5] F. Passerini and A. M. Tonello, "Smart grid monitoring using power line modems: Anomaly detection and localization," *IEEE Transactions on Smart Grid*, vol. 10, no. 6, pp. 6178–6186, 2019.

[6] A. Sendin, I. Peña, and P. Angueira, "Strategies for power line communications smart metering network deployment," *Energies*, vol. 7, no. 4, pp. 2377–2420, 2014. [Online]. Available: https://www.mdpi.com/1996-1073/7/4/2377

[7] V. Taylor and M. Faulkner, "Line monitoring and fault location using spread spectrum on power line carrier," *IEE Proceedings-Generation, Transmission and Distribution*, vol. 143, no. 5, pp. 427–434, 1996.

[8] A. N. Milioudis, G. T. Andreou, and D. P. Labridis, "Enhanced protection scheme for smart grids using power line communications techniques—part II: Location of high impedance fault position," *IEEE Transactions on Smart Grid*, vol. 3, no. 4, pp. 1631–1640, 2012.

[9] M. Bindi, A. Luchetta, G. M. Lozito, C. F. M. Carobbi, F. Grasso, and M. C. Piccirilli, "Frequency characterization of medium voltage cables for fault prevention through multi-valued neural networks and power line communication technologies," *IEEE Transactions on Power Delivery*, vol. 38, no. 5, pp. 3227–3237, 2023.

[10] L. Förstel and L. Lampe, "Grid diagnostics: Monitoring cable aging using power line transmission," in *IEEE Int. Symp. Power Line Commun. and its Appl. (ISPLC)*, 2017, pp. 1–6.

[11] A. Kaushik, Y.C. Eldar, and O.A. Dobre, "Sensing, communications or sensing and communications? perhaps both together," *IEEE Communications Society Technology News (CTN)*, Apr. 2023. [Online]. Available: https://www.comsoc.org/publications/ctn/sensing-communications-or-sensing-and-communications-perhaps-both-together

[12] R. Wonnacott, D. S. Ching, J. Chilleri, C. Safta, L. Rashkin, and T. A. Reichardt, "Industrial PLC network modeling and parameter identification using sensitivity analysis and mean field variational inference," *Sensors*, vol. 23, no. 5, 2023.

[13] F. Passerini and A. M. Tonello, "Smart grid monitoring using power line modems: Effect of anomalies on signal propagation," *IEEE Access*, vol. 7, pp. 27 302–27 312, 2019.

[14] H. V. Poor, *An Introduction to Signal Detection and Estimation (2nd Ed.)*. Berlin, Heidelberg: Springer-Verlag, 1994.

[15] P. Kumari, S. A. Vorobyov, and R. W. Heath, "Adaptive virtual waveform design for millimeter-wave joint communication–radar," *IEEE Transactions on Signal Processing*, vol. 68, pp. 715–730, 2020.

[16] C. Paul, *Analysis of Multiconductor Transmission Lines, Second Edition*. John Wiley & Sons, 2008. [Online]. Available: https://books.google.ca/books?id=833dzQEACAAJ

[17] A. G. Baydin, B. A. Pearlmutter, A. A. Radul, and J. M. Siskind, "Automatic differentiation in machine learning: a survey," *Journal of Machine Learning Research*, vol. 18, no. 153, pp. 1–43, 2018. [Online]. Available: http://jmlr.org/papers/v18/17-468.html

[18] L. W. Yonge, J. Abad, K. H. Afkhamie, L. Guerrieri, S. Katar, H. Lioe, P. Pagani, R. Riva, D. M. Schneider, and A. Schwager, "An overview of the HomePlug AV2 technology," *J. Electr. Comput. Eng.*, vol. 2013, pp. 892 628:1–892 628:20, 2013.

[19] G. Prasad, L. Lampe, and S. Shekhar, "In-band full duplex broadband power line communications," *IEEE Transactions on Communications*, vol. 64, no. 9, pp. 3915–3931, 2016.

[20] D. Bueche, P. Corlay, M. Gazalet, and F.-X. Coudoux, "A method for analyzing the performance of comb-type pilot-aided channel estimation in power line communications," *IEEE Transactions on Consumer Electronics*, vol. 54, no. 3, pp. 1074–1081, 2008.

[21] J. A. Cortés, F. J. Cañete, and L. Díez, "Channel estimation for ofdm-based indoor broadband power line communication systems," *Journal of Communications and Networks*, vol. 25, no. 2, pp. 151–166, 2023.

[22] V. Nagesha and S. Kay. (1992) Cramer-Rao lower bounds for complex parameters. Accessed 2022. [Online]. Available: https://www.ele.uri.edu/faculty/kay/New%20web/downloadable%20files/Nageha_complex%20CRLB.pdf

[23] R. F. H. Fischer, *Precoding and signal shaping for digital transmission*. John Wiley & Sons, 2005.